Clusteromics IV: The Role of Nitric Acid in Atmospheric Cluster Formation

Yosef Knattrup and Jonas Elm*

Read Online

ACCESS | Metrics & More | Article Recommendations | Supporting Information

ABSTRACT: Nitric acid (NA) has previously been shown to affect atmospheric new particle formation; however, its role still remains highly uncertain. Through the employment of state-of-the-art quantum chemical methods, we study the $(acid)_{1-2}(base)_{1-2}$ and $(acid)_3(base)_2$ clusters containing at least one nitric acid (NA) and sulfuric acid (SA) or methanesulfonic acid (MSA) with bases ammonia (A), methylamine (MA), dimethylamine (DMA), trimethylamine (TMA), and ethylenediamine (EDA). The initial cluster configurations are generated using the ABCluster program. PM7 and ωB97X-D/6-31++G(d,p) calculations are used to reduce the number of relevant configurations. The thermochemical parameters are calculated at the ωB97X-D/6-31++G(d,p) level of theory with the quasi-harmonic approximation, and the final single-point energies are calculated with high-level DLPNO−CCSD(T$_0$)/aug-cc-pVTZ calculations. The enhancing effect from the presence of nitric acid on cluster formation is studied using the calculated thermochemical data and cluster dynamics simulations. We find that when NA is in excess compared with the other acids, it has a substantial enhancing effect on the cluster formation potential.
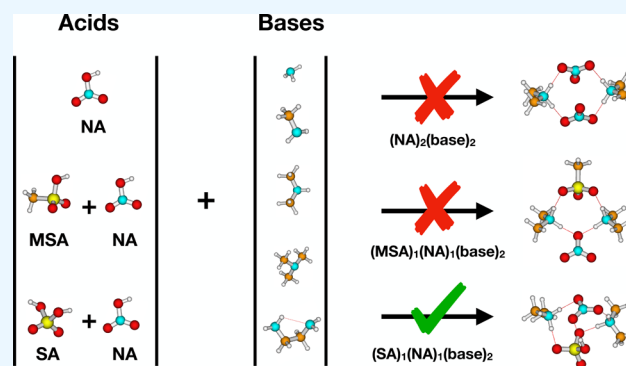
1. INTRODUCTION

Aerosols are nano- to microscale particles, which have pronounced effects on our global climate. Aerosols affect the global radiation balance by the scattering of sunlight[1] and aerosols have the potential to act as seeds for cloud droplet formation.[2] Atmospheric new particle formation (NPF) is primarily driven by the clustering of atmospheric low volatile acids with bases, and NPF has been shown to make up roughly half of cloud condensation nuclei (CCN).[3] However, the largest uncertainty in global climate estimation is due to uncertainties of the compounds involved in the formation and growth of aerosols.[4] It is known that sulfuric acid (SA, H_2SO_4) plays a major role in NPF[5−8] and that methanesulfonic acid (MSA, CH_3SO_3H) is capable of enhancing the cluster formation potential of SA-based clusters.[9,10] Nitric acid (NA, HNO_3) is a potential precursor for aerosols and is formed as a termination product of the NO_x cycle of petrochemical smog formation, as well as in fossil fuel combustion and other natural and anthropogenic processes.[11] NA can be highly abundant in the gas phase and reach concentrations on the order of 10^{12} molecules cm^{-3} in the polluted troposphere.[12] This is several orders of magnitude higher than SA and MSA, which usually are found in concentrations ranging from 10^5 to 10^7 molecules cm^{-3}.[5,13−15]

Wang et al.[16] studied mixtures of NA and ammonia (A, NH_3) vapors under atmospheric conditions in the CLOUD chamber at CERN. It was found that below temperatures of

278.5 K the vapors of NA and A condense onto freshly nucleated particles and that for temperatures below 258.15 K nucleation of NA and A vapors to ammonium nitrate particles happen directly through an acid−base stabilization mechanism. Wang et al. postulated that under most urban conditions SA and an available base will cause the initial nucleation and early growth up to the activation size, which forms a core for NA and A vapors to condense onto. Very recently, Wang et al.[17] further extended their study and showed at the CLOUD chamber that NA, SA, and A could synergistically form particles in the upper free troposphere (at $T = 223$ K and 25% relative humidity). Despite its high abundance and potential as a nucleation precursor, the exact role of NA in NPF is still uncertain. This is because field measurements of NPF usually use the nitrate ion (NO_3^-) as the chemical ionization reagent, which could mask the presence of NA in the cluster.[18] Furthermore, measurement of the initial steps in cluster formation using experimental setups with mass spectrometry can be problematic because it is uncertain if the cluster

measured is the one initially formed or a cluster formed by fragmentation inside the instrument.[19,20]

Quantum chemical calculations can yield insight into cluster formation, but studies involving NA remain scarce compared with the extensively studied SA−base[21−33] and MSA−base[34−45] cluster systems. One of the first quantum chemical studies involving NA was performed by Nguyen et al.,[46] who studied the $(NA)_1(A)_1$ dimer cluster at the MP2/6-311++G(d,p) level of theory. It was found that the ion-pair ammonium nitrate structure was stabilized when applying a water polarizable continuum model (PCM), but the ion-pair was highly unstable on the potential energy surface in the gas phase. Tao[47] extended the work by studying the role of explicit water molecules (W, H_2O) in the $(NA)_1(A)_1(W)_n$ clusters, for $n = 0−3$ using MP2/6-311++G(d,p) for $n = 0, 1$ and MP2/6-31+G(d) for $n = 2, 3$. Tao found that the clusters required at least two water molecules to facilitate the proton transfer from NA to A.

Ling et al.[48] studied the $(NA)_m(A)_n$ clusters at the B3LYP-D3/6-311++G(d,p) level of theory for all combinations of clusters satisfying $m, n \leq 4$ or $m = n$ for $m, n = 5, ..., 8$. They found that proton transfer is generally preferred except for the smallest clusters, and the clusters generally were stabilized by the formation of hydrogen-bonded networks. The binding free energies showed that it is the most thermodynamically favorable to grow through the $m = n$ structures via the addition of an acid and then a base. A similar mechanism has been shown for SA−base clusters.[9,31,49] Evaporation rates were calculated by considering the detailed balance for reactions between molecules or molecular clusters. They found that the $m = n$ clusters are more stable than similar-sized clusters and that the evaporation rate almost decreases monotonously when going from the $(NA)_1(A)_1$ to the $(NA)_8(A)_8$ system.

More recent studies have also looked into the cluster dynamics of clusters containing NA. Kumar et al.[50] studied the $(NA)_{1−3}(A)_{1−3}(W)_{0−2}$ clusters at the M06-2X/aug-cc-pVTZ level of theory. Using the Atmospheric Cluster Dynamic Code (ACDC), they investigated particle formation from NA and A under different relative humidity conditions (0−100%). It was identified that the possible gas-phase clusters were $(NA)_3(A)_2$, $(NA)_3(A)_3$, and $(NA)_4(A)_3$, which formed through different growth mechanisms under different relative humidity conditions.

Liu et al.[51] extended the cluster systems to study mixed $(acid)_m(A)_n$ clusters for $0 \leq n \leq m \leq 3$, where the acids were NA and SA at the M06-2X/6-311++G(3df,3pd) level of theory. It was shown that NA forms clusters with SA and A through hydrogen-bonded interactions and that, for most of the clusters, proton transfer occurred. The cluster formation potential and mechanism were calculated using ACDC at extremely cold temperatures of 220 and 240 K. They found the enhancement by NA for the cluster formation potential was biggest for a high concentration of NA and A, a low concentration of SA, and colder temperatures. For the most favorable conditions, the addition of NA could enhance the cluster formation potential up to 6 orders of magnitude. For the mechanism, Liu et al.[51] found that NA acted as a "bridge" connecting smaller and larger clusters by adding to the smaller clusters, letting the cluster grow and then NA would evaporate at larger cluster sizes. A few years later Liu et al.[18] extended their work by studying the $(SA)_x(NA)_y(DMA)_z$ clusters for $0 \leq z \leq (x + y) \leq 3$ at the RI-CC2/aug-cc-pV(T+d)Z//M06-2X/6-311++G(3df,3pd) level of theory. They calculated the

cluster formation mechanism using ACDC at temperatures of 260 and 280 K. It was found that with concentrations of NA up to 10^{11} molecules cm^{-3}, NA could enhance the SA-DMA cluster formation potential up to 80-fold for cold and polluted areas and at 280 K NA contributed to 75% of the cluster formation pathways.[18]

While NA-containing clusters have received increasing attention in recent years, multicomponent clusters involving a combination of both SA, MSA, and NA and different bases have still not been studied to date. This work is the fourth paper in the clusteromics series[9,10,52] where the thermodynamics and kinetics of the initial steps in cluster formation are studied. Here, we report the thermodynamic and cluster growth kinetics of $(acid)_{1−2}(base)_{1−2}$ and $(acid)_3(base)_2$ clusters containing at least one nitric acid (NA) and where the other acids are sulfuric acid (SA) or methanesulfonic acid (MSA) and the bases are ammonia (A), methylamine (MA), dimethylamine (DMA), trimethylamine (TMA), and ethylenediamine (EDA).

2. COMPUTATIONAL DETAILS

Gaussian 16[53] was used for the semiempirical PM7[54] and density functional theory (DFT) geometry optimization and vibrational frequency calculations. The Gaussian 09 default convergence criteria [corresponding to Integral = (FineGrid,Acc2E = 10)] were used to match the level of theory with the current data in the Atmospheric Cluster Database (ACDB).[55] ORCA 4.2.1[56,57] was used to calculate the single point energies using the domain-based local pair natural orbital method DLPNO−CCSD(T_0)[58,59] with a TightSCF convergence criterion[60] and the aug-cc-pVTZ basis set. The ωB97X-D functional[61] and the 6-31++G(d,p) basis set[62,63] was employed at the DFT level on the basis of multiple benchmarks[64−66] for atmospheric relevant clusters. When calculating binding energies, the presence of basis set superposition errors (BSSE) can be of concern. We have previously shown for atmospheric molecular clusters that when using medium-sized basis sets, the uncorrected binding energies show better agreement with the complete basis set limit compared with the counterpoise-corrected binding energies.[63,65] Hence, we do not correct for BSSE in our binding energy calculations.

Grimme's quasi-harmonic approximation[67] was used to treat vibrational frequencies below 100 cm^{-1} using the Goodvibes[68] code. The cluster structures were sampled using a funneling workflow[69−71] in accordance with the previous clusteromics papers.[9,10,52] The workflow will briefly be outlined here, but for a more in-depth outline, we refer to our recent review and papers.[9,10,52,72]

ABCluster → PM7 → sort → DFT → restart → sort

→ inspection → DLPNO

The initial calculations with ABCluster[73,74] used the recommended settings by Kubečka et al.[70] corresponding to SN = 3000 as the population size, $g_{max} = 200$ as the maximum amount of generations, and $g_{limit} = 4$ as the number of scout bees. Because the CHARMM force field is not capable of simulating proton transfer reactions, 1000 local minima were saved for each cluster protonation state by using neutral, anionic, and cationic monomers. ArbAlign[75] was used for the sorting stage to remove identical cluster configurations on the basis of root-mean-square deviations (RMSD) between atomic positions. An RMSD cutoff of 0.38 Å was applied on the basis
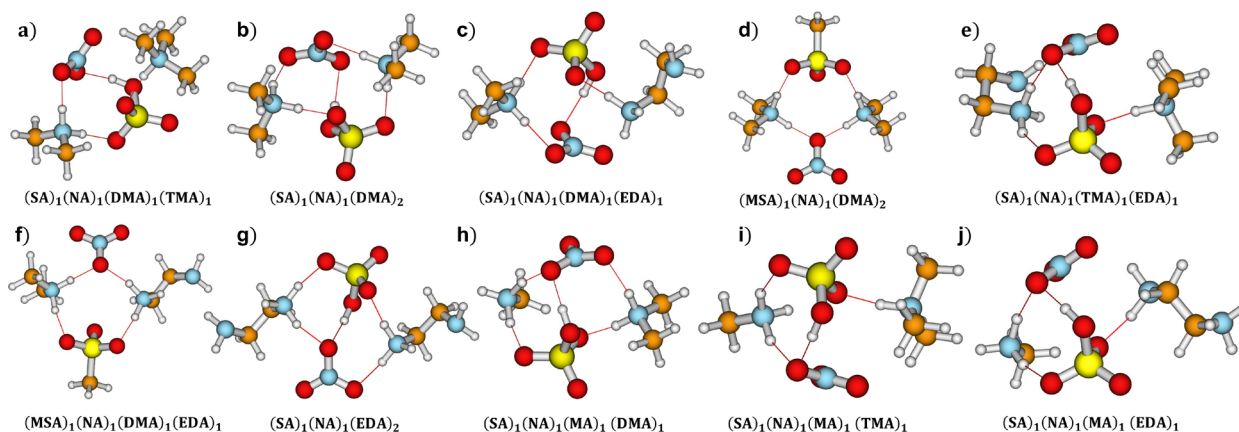
Figure 1. (a−j) Clusters with the lowest binding free energy at the DLPNO−CCSD(T_0)/aug-cc-pVTZ//ωB97X-D/6-31++G(d,p) level of theory. Calculated with the quasi-harmonic approximation at 298.15 K and 1 atm. Yellow = sulfur, blue = nitrogen, red = oxygen, brown = carbon, and white = hydrogen.

Table 1. Calculated Binding Free Energies (kcal/mol) at the DLPNO−CCSD(T_0)/aug-cc-pVTZ//ωB97X-D/6-31++G(d,p) Level of Theory with the Quasi-Harmonic Approximation at 298.15 K and 1 atm

	classification	$(SA)_1(NA)_1$	$(MSA)_1(NA)_1$	$(NA)_1$	$(NA)_2$
$(A)_1$	w	−5.4	−6.0	−3.0	1.4
$(MA)_1$	m	−13.7	−11.3	−3.6	−3.7
$(DMA)_1$	s	−17.3	−15.2	−4.7	−7.7
$(TMA)_1$	s	−18.8	−15.7	−4.9	−8.6
$(EDA)_1$	s	−17.1	−14.5	−4.0	−7.4
$(A)_2$	w, w	−14.3	−13.3	2.8	−5.4
$(MA)_2$	m, m	−23.7	−23.3	−0.8	−15.6
$(DMA)_2$	s, s	−32.7	−30.9	−5.3	−24.5
$(TMA)_2$	s, s	−26.9	−19.8	−1.8	−15.3
$(EDA)_2$	s, s	−29.1	−27.3	−4.5	−20.0
$(A)_1(MA)_1$	w, m	−20.3	−18.5	−0.9	−11.0
$(A)_1(DMA)_1$	w, s	−23.7	−22.0	−4.2	−15.3
$(A)_1(TMA)_1$	w, s	−22.9	−17.2	−1.9	−11.3
$(A)_1(EDA)_1$	w, s	−22.4	−20.3	−2.8	−13.1
$(MA)_1(DMA)_1$	m, s	−29.1	−26.9	−4.5	−20.7
$(MA)_1(TMA)_1$	m, s	−27.6	−22.9	−1.1	−15.8
$(MA)_1(EDA)_1$	m, s	−27.4	−25.1	−3.0	−18.3
$(DMA)_1(TMA)_1$	s, s	−32.9	−25.7	−4.7	−20.0
$(DMA)_1(EDA)_1$	s, s	−32.4	−29.3	−6.4	−22.0
$(TMA)_1(EDA)_1$	s, s	−29.9	−24.1	−3.2	−19.2

of previous studies[76,77] of atmospherically relevant clusters. The remaining structures were optimized at the DFT level, restarted until convergence, and sorted using ArbAlign. The five cluster structures with the lowest free energy at the DFT level had their single point energies calculated at the DLPNO−CCSD(T_0)/aug-cc-pVTZ level of theory.

2.1. ACDC. The Atmospheric Cluster Dynamics Code (ACDC)[78,79] was used to simulate the cluster formation potential ($J_{potential}$) using the calculated thermochemical parameters ΔH and ΔS as inputs. ACDC simulates the cluster steady-state concentrations (c_i) using the following birth−death equation:

$$\frac{dc_i}{dt} = \sum_{j<i} \beta_{j,(i-j)} c_j c_{(i-j)} + \sum_j \gamma_{(i+j) \to i} c_{i+j} - \sum_j \beta_{i,j} c_i c_j - \sum_{j<i} \gamma_{i \to j} c_i + Q_i - S_i$$

(1)

Here, $\beta_{i,j}$ is the collision coefficient between the clusters i and j and $\gamma_{i \to j}$ is the evaporation coefficient of cluster i into two smaller fragments j and $(i - j)$. Q_i is an external concentration source, and S_i is the coagulation loss of clusters i. The cluster formation ($J_{potential}$) is the flux toward relevant larger clusters for the given input system and it estimates the potential for smaller clusters to grow into larger sizes. It is calculated as the sum of clusters growing out of the system. Likewise, clusters consisting of $(acid)_3(base)_{2-3}$ were allowed to leave the simulation box. The $(acid)_2(base)_3$ clusters were disabled as contributors to $J_{potential}$ because clusters with more bases than acids usually are unstable in electrically neutral acid−base cluster systems.[31,79] The original ACDC code was downloaded from the ACDC repository[79−81] and modified. Default values for size dependent coagulation loses were used (cs_exp = −1.6 and cs_ref = 1×10^{-3}) to match typical values in the boundary layer. The simulations were performed at 278.15 K in accordance with our previous papers,[9,10,52] which corresponds to springtime in the boreal forest environment.

3. RESULTS AND DISCUSSION

3.1. Cluster Structures. Using the workflow described above we identified a total of 21 379 unique $(acid)_{1-2}(base)_{1-2}$ and $(acid)_3(base)_2$ cluster structures at the ωB97X-D/6-31++G(d,p) level of theory containing at least one NA. All the cluster structures and thermochemistry have been added to the Atmospheric Cluster Database (ACDB).[55] The 10 $(acid)_{1-2}(base)_{1-2}$ cluster systems with the lowest binding free energy at the $DLPNO-CCSD(T_0)/aug\text{-}cc\text{-}pVTZ//$ ωB97X-D/6-31++G(d,p) level of theory are shown in Figure 1. The structures of the 10 $(acid)_3(base)_2$ cluster systems lowest in free energy are shown in the Supporting Information.

The identified clusters show that the most stable clusters contain several hydrogen-bonded interactions and have undergone an acid–base reaction between all acids and bases in the system. As can be seen in the $(SA)_1(NA)_1(DMA)_1(TMA)_1$ cluster (Figure 1a), the proton transfer is between the acid–base pair of the same strength. The acid–base pair trend is consistent within the remaining clusters not depicted here. In our previous studies,[9,10] we found that the SA-based clusters primarily were held together via direct bisulfate–bisulfate interactions, in contrast to the MSA-based clusters where MSA's methyl group and the proton transfers from the MSA molecules to the bases make the clusters unable to exhibit direct acid–acid interactions. This forces the MSA-based clusters to be held together by linking the acids via the bases. When exchanging one of the acids with NA, the interaction patterns follow the same trend as the pure acid clusters, because a direct bisulfate–nitrate interaction can be seen in the SA–NA–base clusters, but not in the MSA–NA–base clusters. In general, the SA-containing clusters are often more stable than the systems with only MSA or only NA. This is clear because the former two systems only make up 2 and 0 of the 10 most stable $(acid)_{1-2}(base)_{1-2}$ clusters depicted in Figure 1, respectively. Clustering with the stronger bases yields the most stable structures. This can be seen by MA first showing up once most of the combinations of EDA, DMA, and TMA have been used. Like the previously studied mixed SA–MSA–base clusters,[52] the most stable clusters are generally not symmetrical. However, the previously identified SA–base clusters[9] generally adopted an unsymmetrical shape, and the MSA–base clusters[10] adopted a symmetrical shape. The addition of NA does not seem to change this trend as the two symmetrical clusters in Figure 1 are the clusters with MSA, and the remaining unsymmetrical clusters are the clusters containing SA.

3.2. Thermochemistry. Table 1 presents the calculated binding free energies for the $(acid)_{1-2}(base)_{1-2}$ clusters at the $DLPNO-CCSD(T_0)/aug\text{-}cc\text{-}pVTZ//\omega$B97X-D/6-31++G-(d,p) level of theory, with the quasi-harmonic approximation at 298.15 K and 1 atm.

On the basis of the gas phase basicity,[82] the bases are divided into three classifications: weak (A), medium (MA), and strong (DMA, TMA, and EDA). The $(acid)_{1-2}(base)_1$ clusters all show the same trend for the most negative binding free energies: $(A)_1 < (MA)_1 < (EDA)_1 < (DMA)_1 < (TMA)_1$. There is a clear trend between basicity and large negative binding free energy. However, the trend is not directly proportional since EDA and DMA are flipped between the trend and the basicity ranking. This is likely because DMA contains secondary amino groups, while EDA contains two primary amino groups, which require a larger cluster to obtain

its full potential. The $(acid)_{1-2}(base)_2$ clusters with the same two bases present two trends: the $(SA)_1(NA)_1(base)_2$ and $(NA)_1(base)_2$ clusters follow $(A)_2 < (MA)_2 < (TMA)_2 < (EDA)_2 < (DMA)_2$, while the $(MSA)_1(NA)_1(base)_2$ and $(NA)_2(base)_2$ clusters follow $(A)_2 < (TMA)_2 < (MA)_2 < (EDA)_2 < (DMA)_2$. The clusters roughly follow the previous trend, but TMA has become more unfavorable because its three methyl groups are quite bulky, and steric hindrance is preventing the cluster from obtaining a more favorable structure. TMA also has the disadvantage of lower hydrogen bond capacity, as it only has the ability to accept a single proton and, therefore, it can only act as a single hydrogen-bond donor. The $(acid)(A)_1(base)_1$ clusters follow $(MA)_1 < (EDA)_1 < (TMA)_1 < (DMA)_1$ for $(SA)(NA)$, $(TMA)_1 < (MA)_1 < (EDA)_1 < (DMA)_1$ for $(MSA)_1(NA)_1$, and $(MA)_1 < (TMA)_1 < (EDA)_1 < (DMA)_1$ for $(NA)_{1-2}$. Steric hindrance and hydrogen-bond capacity of the bases are now the defining factors for the trends. These defining factors still hold for larger clusters where there is a general affinity for DMA and EDA and an aversion for TMA, as can be seen in the $(acid)$-$(MA)_1(base)_1$ clusters which follow $(EDA) < (TMA) < (DMA)$ for $(SA)_1(NA)_1$ and $(TMA) < (EDA) < (DMA)$ for the rest. The trend can also be seen in the clusters consisting of strong base combinations, which follow $(TMA)_1(EDA)_1 < (DMA)_1(EDA)_1 < (DMA)_1(TMA)_1$ for $(SA)(NA)$ and $(TMA)_1(EDA)_1 < (DMA)_1(TMA)_1 < (DMA)_1(EDA)_1$ for the rest. Overall, except for the $(SA)_1(NA)_1(A)_1$ cluster, the SA-containing clusters always have a more negative binding free energy compared with their MSA counterparts. Both are much more negative compared with the clusters that only contain NA as the acid. The overall trend is that stronger bases result in a more negative binding free energy, but this is not true within the different subsystems, as shown before. Here, the acid–base interactions seem to dominate for the smaller clusters system, but as soon as steric hindrance and lack of hydrogen-bond capacity become a dominating factor, a preference for DMA and EDA and an aversion for TMA, which suffers from both problems, shows in all the systems. The strongest bonded clusters are thus those containing DMA and/or EDA, which is consistent with previous studies.[9,10,52] It should be noted that mixed base clusters will most likely be more important than the clusters with only one type of base, due to the increased available vapor concentration, under the premise that their thermochemistry is similar. Hence, clusters that consist of both DMA and EDA will most likely be more favorable than the clusters that contain only DMA or EDA.[9,10,83]

The gain in free energy when adding another molecule to the clusters was studied by calculating the addition free energies of NA/SA to the $(SA)(base)_{1-2}$ clusters, NA/MSA to $(MSA)(base)_{1-2}$ clusters, and NA to the $(NA)_2(base)_{1-2}$ clusters. The results are presented in Table 2. The calculations are performed at the $DLPNO-CCSD(T_0)/aug\text{-}cc\text{-}pVTZ//$ ωB97X-D/6-31++G(d,p) level of theory with the quasi-harmonic approximation (298.15 K, 1 atm).

The results show that there is a preference for adding the same acid to a given cluster compared with adding NA and that it is always favorable to add another acid, with the exception of adding NA to the $(SA)_1(A)_1$ or $(NA)_1(A)_1$ clusters. The addition free energy of adding NA to MSA-based clusters is always more favorable than adding NA to SA-based clusters. The studied systems were expanded to include $(acid)_3(base)_2$ cluster structures containing at least one NA to

Table 2. Addition Free Energies (kcal/mol) at the DLPNO−CCSD(T_0)/aug-cc-pVTZ//ωB97X-D/6-31++G(d,p) Level of Theory with the Quasi-Harmonic Approximation at 298.15 K and 1 atm[a]

initial cluster	(SA)		(MSA)		(NA)
added acid	(SA)[9]	(NA)	(MSA)[10]	(NA)	(NA)
(A)$_1$	−13.8	0.2	−9.0	−2.6	4.4
(MA)$_1$	−17.2	−6.5	−13.9	−7.4	−0.1
(DMA)$_1$	−17.9	−5.8	−14.5	−8.1	−3.0
(TMA)$_1$	−15.3	−6.2	−10.4	−7.0	−3.7
(EDA)$_1$	−17.7	−6.7	−15.7	−7.4	−3.4
(A)$_2$	−17.3	−4.6	−17.9	−10.7	−8.2
(MA)$_2$	−25.9	−13.0	−24.1	−15.9	−14.8
(DMA)$_2$	−29.1	−17.8	−24.6	−18.9	−19.2
(TMA)$_2$	−26.2	−11.6	−19.6	−13.8	−13.5
(EDA)$_2$	−25.5	−12.8	−21.5	−14.4	−15.5
(A)$_1$(MA)$_1$	−22.4	−10.3	−19.4	−11.8	−10.1
(A)$_1$(DMA)$_1$	−21.3	−10.3	−23.6	−16.7	−11.1
(A)$_1$(TMA)$_1$	−18.7	−9.3	−15.5	−9.6	−9.4
(A)$_1$(EDA)$_1$	−20.9	−9.6	−18.2	−11.2	−10.3
(MA)$_1$(DMA)$_1$	−26.4	−14.9	−23.1	−16.2	−16.2
(MA)$_1$(TMA)$_1$	−24.7	−14.2	−20.7	−15.5	−14.7
(MA)$_1$(EDA)$_1$	−25.7	−14.0	−22.5	−15.4	−15.3
(DMA)$_1$(TMA)$_1$	−27.5	−18.1	−20.7	−15.7	−15.3
(DMA)$_1$(EDA)$_1$	−26.0	−15.0	−24.7	−18.6	−15.6
(TMA)$_1$(EDA)$_1$	−27.6	−14.8	−21.3	−15.8	−16.0

[a]Calculated as the initial cluster binding free energy subtracted from the binding free energy of the cluster with the added acid. The non-NA cluster data is from our previous studies.[9,10]

investigate if this trend is valid for larger systems. The calculated binding free energies for these systems can be seen in Table 3.

All the clusters have highly negative binding free energies. The (SA)$_2$(NA)$_1$-based clusters are the most favorable, followed by (SA)$_1$(MSA)$_1$(NA)$_1$ and then (MSA)$_2$(NA)$_1$. In terms of trends, clustering with a stronger base (based on the classifications s, m, and w) yields a lower binding free energy. The clusters are already at a size where the sterical hindrance and hydrogen bond capacity are the dominating factors and

the preference for DMA and EDA and aversion for TMA can be seen again, especially for the clusters containing MSA.

The addition free energy for the larger systems is shown in Table 4. Compared with the smaller clusters, the addition of an

Table 4. Addition Free Energies (kcal/mol) at the DLPNO−CCSD(T_0)/aug-cc-pVTZ//ωB97X-D/6-31++G(d,p) Level of Theory with the Quasi-Harmonic Approximation at 298.15 K and 1 atm

initial cluster:	(SA)$_2$[9]	(MSA)$_2$[10]	(SA)$_1$(MSA)$_1$[52]
added acid:	(NA)	(NA)	(NA)
(A)$_2$	−4.3	−5.9	−6.2
(MA)$_2$	−5.1	−4.7	−6.1
(DMA)$_2$	−6.0	−4.7	−6.0
(TMA)$_2$	−2.6	−6.2	−7.5
(EDA)$_2$	−4.5	−6.6	−8.1
(A)$_1$(MA)$_1$	−3.8	−5.1	−5.9
(A)$_1$(DMA)$_1$	−7.2	−5.5	−6.7
(A)$_1$(TMA)$_1$	−7.3	−8.3	−4.9
(A)$_1$(EDA)$_1$	−6.0	−7.3	−4.5
(MA)$_1$(DMA)$_1$	−6.1	−5.6	−6.1
(MA)$_1$(TMA)$_1$	−7.0	−5.8	−5.7
(MA)$_1$(EDA)$_1$	−5.7	−6.1	−5.4
(DMA)$_1$(TMA)$_1$	−3.8	−8.3	−6.1
(DMA)$_1$(EDA)$_1$	−5.1	−6.3	−5.3
(TMA)$_1$(EDA)$_1$	−5.9	−10.4	−11.9

acid is still favorable, but the gain in free energy is lower and more evenly distributed among the possible acid additions. The preference for adding NA to the MSA clusters is no longer present, except for the (base)$_2$ clusters where the addition of NA to (SA)$_1$(MSA)$_1$ gives the highest gain, while for the (A)$_1$(base)$_1$ cluster the addition of NA to the (MSA)$_2$ results in the highest gain. The exception is (A)$_1$(DMA)$_1$, where the addition of (NA) to (SA)$_2$ is preferred. For the larger systems, there is no clear trend. However, NA addition free energy is, in general, seen to be in the range from −2.6 to −11.9 kcal/mol, with an average value of −6.08 kcal/mol.

3.3. Cluster Formation Potential. Because NA can be found in high concentrations, its abundance might drive the formation potential of the clusters. We have used ACDC to

Table 3. Calculated Binding Free Energies (kcal/mol) at the DLPNO−CCSD(T_0)/aug-cc-pVTZ//ωB97X-D/6-31++G(d,p) Level of Theory with the Quasi-Harmonic Approximation at 298.15 K and 1 atm

	classification	(SA)$_2$(NA)$_1$	(MSA)$_2$(NA)$_1$	(SA)$_1$(MSA)$_1$(NA)$_1$
(A)$_2$	w, w	−31.3	−26.4	−29.8
(MA)$_2$	m, m	−41.7	−36.2	−39.9
(DMA)$_2$	s, s	−50.0	−41.3	−47.8
(TMA)$_2$	s, s	−44.1	−31.8	−39.4
(EDA)$_2$	s, s	−46.3	−41.0	−47.2
(A)$_1$(MA)$_1$	w, m	−36.2	−31.2	−35.0
(A)$_1$(DMA)$_1$	w, s	−41.9	−34.4	−39.7
(A)$_1$(TMA)$_1$	w, s	−39.6	−31.4	−34.5
(A)$_1$(EDA)$_1$	w, s	−39.7	−34.6	−36.7
(MA)$_1$(DMA)$_1$	m, s	−46.7	−39.4	−44.5
(MA)$_1$(TMA)$_1$	m, s	−45.1	−33.9	−41.3
(MA)$_1$(EDA)$_1$	m, s	−44.8	−38.3	−42.1
(DMA)$_1$(TMA)$_1$	s, s	−46.1	−39.0	−44.6
(DMA)$_1$(EDA)$_1$	s, s	−48.5	−41.7	−46.0
(TMA)$_1$(EDA)$_1$	s, s	−48.6	−40.0	−47.5

simulate the cluster formation potential ($J_{potential}$) for the NA–SA–base and NA–MSA–base systems. The concentration of SA and MSA was set to 1×10^6 molecules cm^{-3} and NA was set to 2.46×10^{11} molecules cm^{-3}. The bases were set to the following atmospherically relevant ranges of mixing ratios: A (10 ppt–10 ppb), MA (1–100 ppt), DMA (1–10 ppt), TMA (1–10 ppt), and EDA (1–10 ppt). The simulated system can be seen as an $m \times n$ box, where m is the number of acids and n is the number of bases. The sum of fluxes out of this box can be seen as the potential for the cluster to grow into a larger size and contribute to new particle formation. It has been shown[31,79] that acid–base clusters are most stable along the diagonal on the acid–base cluster grid and that the $(acid)_{1-2}(base)_{1-2}$ clusters are the limiting steps for new particle formation. Thus, our simulation is limited to a box size of 2×2, where the $(acid)_3(base)_2$ and $(acid)_3(base)_3$ clusters are the only ones allowed to leave the box and contribute to $J_{potential}$. Table 5 lists the simulated cluster formation potentials. The simulations were performed using the calculated thermochemistry at 278.15 K.

Table 5. Simulated Cluster Formation Potential ($J_{potential}$, cm^{-3} s^{-1}) for the Nitric-Acid-Based Clusters Containing a Single Type of Base, with Simulations Performed at 278.15 K

cluster system	lower limit	upper limit
ammonia (A)	10 ppt	10 ppb
NA–SA–A	3.35×10^{-5}	8.15×10^{-1}
NA–MSA–A	1.26×10^{-7}	1.25×10^{-1}
methylamine (MA)	1 ppt	100 ppt
NA–SA–MA	8.69×10^{-4}	1.87
NA–MSA–MA	5.35×10^{-5}	5.27×10^{-1}
dimethylamine (DMA)	1 ppt	10 ppt
NA–SA–DMA	1.48	25.0
NA–MSA–DMA	1.04×10^{-2}	9.93×10^{-1}
trimethylamine (TMA)	1 ppt	10 ppt
NA–SA–TMA	9.83	92.5
NA–MSA–TMA	2.91×10^{-5}	2.91×10^{-3}
ethylenediamine (EDA)	1 ppt	10 ppt
NA–SA–EDA	3.27×10^{-1}	10.7
NA–MSA–EDA	2.88×10^{-3}	2.16×10^{-1}

The potentials for the NA–MSA clusters are essentially zero or very low in the lower concentration limit regime and is therefore not expected to drive cluster formation. In the upper concentration limit regime, the cluster formation potential for these systems increases at least 4 orders of magnitude to more influential values, albeit they are still quite low. This is likely due to MSA-based clusters not being able to bond as strongly as SA because of the lack of bisulfate–nitrate interactions. Similarly, the potentials for NA–SA–A, NA–SA–MA and NA–SA–EDA are quite low in the lower concentration limit regime, but unlike the MSA clusters, they are more substantial in the upper concentration limit regime. For instance, for the NA–SA–EDA cluster system, the cluster formation potential increases to 10.7 cm^{-3}s^{-1} in the high concentration limit. This could indicate that NA–SA–EDA clusters could potentially be formed and grow under the given atmospheric conditions. The major contributors to the potentials for both regimes are the NA–SA–DMA and NA–SA–TMA clusters and they will, therefore, be the main clusters that will be formed and grow under relevant atmospheric conditions. The trend for a larger

$J_{potential}$ (A) is: < (MA) < (EDA) < (DMA) < (TMA), which is the same trend as the most negative binding free energy for the $(acid)_{1-2}(base)_1$ clusters, which hints at the fact that the small clusters, and by extension the basicity of the base, are the determining factor for the cluster formation potential.

Nearly all the clusters leave the simulation box via cluster–NA monomer collisions (see Supporting Information, Table S1). This is because the concentration of NA is a lot higher than the other acids, which makes it the most likely acid monomer to collide with. The exceptions are the NA–MSA–A and NA–MSA–TMA clusters, which leave the box via cluster–cluster collisions; however, these were the systems with low $J_{potential}$ and are, therefore, not an important mechanism. The clusters with substantial $J_{potential}$, NA–SA–MA and NA–SA–EDA in the upper concentration limit regime and NA–SA–DMA and NA–SA–TMA in both regimes, contain NA in the collision clusters as one of the main fluxes, which shows that NA also has an enhancing effect during the initial cluster growth and not only as the collision partner. Collision clusters containing NA are actually the main contributor to the flux in the NA–SA–DMA and NA–SA–MA systems; however, the systems with the highest $J_{potential}$ have the $(SA)_2(base)_2$ collision cluster as the main contributor to the flux.

3.4. Enhancement in $J_{potential}$. The simulated cluster formation potentials of the NA–SA/MSA–base clusters can be compared with the equivalent SA/MSA-base cluster calculated in Clusteromics III to quantify the enhancing effect when including NA.[52] The enhancement factor is calculated for both the upper and lower concentration limit regime as

$$R_{NA} = \frac{J_{potential}(NA-SA/MSA-base)}{J_{potential}(SA/MSA-base)} \quad (2)$$

The results are presented in Table 6.

In general, the addition of NA always has an enhancing effect on the cluster formation potential. The first thing one notices is the extreme enhancement for most of the systems. This effect, however, is an artifact of dividing two cluster formation potentials that essentially are zero with each other.

Table 6. Enhancement (R_{NA}) in the Simulated Cluster Formation Potential by Having NA Present[a]

cluster system	lower limit	upper limit
ammonia (A)	10 ppt	10 ppb
NA–SA–A	2.66×10^5	6.47×10^3
NA–MSA–A	7.46×10^7	7.40×10^7
methylamine (MA)	1 ppt	100 ppt
NA–SA–MA	1.58×10^2	88.6
NA–MSA–MA	6.16×10^3	6.24×10^3
dimethylamine (DMA)	1 ppt	10 ppt
NA–SA–DMA	2.94	3.74
NA–MSA–DMA	1.54×10^2	3.53×10^2
trimethylamine (TMA)	1 ppt	10 ppt
NA–SA–TMA	18.2	4.22
NA–MSA–TMA	2.06×10^4	2.08×10^6
ethylenediamine (EDA)	1 ppt	10 ppt
NA–SA–EDA	7.64	10
NA–MSA–EDA	1.45×10^3	1.14×10^3

[a]Non-NA data was taken from Clusteromic III.[52] The simulations are performed at 278.15 K

For example, even though there is an enhancement for NA−MSA−A on the order of 10^7 in the lower concentration limit regime, the absolute value of $J_{potential}$ is still on the order of 10^{-7} cm^{-3} s^{-1}. The enhancement for the systems with substantial $J_{potential}$ is in the range of ∼3 for the NA−SA−DMA system up to ∼89 for the NA−SA−MA system. However, this large enhancement is predominantly due to the relatively low cluster formation potential of the SA−MA system. It should be noted that the increase in cluster formation potential is also an effect of increasing the available concentration of acid vapor. The NA concentration of 2.46×10^{11} molecules cm^{-3} (10 ppb) corresponds to extremely polluted areas. The influence of lower concentrations in less polluted areas was studied by running the NA−SA−TMA and NA−SA−DMA systems at NA concentrations of 2.46×10^8 molecules cm^{-3} (10 ppt). For the NA−SA−TMA system, the cluster formation potential reduced to 9.09 cm^{-3} s^{-1} in the lower concentration limit regime and 82 cm^{-3} s^{-1} in the upper concentration limit regime. The lower concentration limit distribution of outgoing clusters stayed the same, but in the upper concentration limit regime, all the outbound clusters changed to the $(SA)_2(base)_2+(NA)_1$ system. For the NA−SA−DMA system, the cluster formation potential reduced to 1.36 and 13.4 cm^{-3} s^{-1} in the lower and upper concentration limit regimes, respectively. The lower and upper concentration limit distributions of outgoing clusters both changed to 99% $(SA)_2(base)_2+(NA)_1$. As can be seen from these results, even lower concentrations of NA still greatly enhance the cluster formation potential when NA is in excess compared with the other acids. Furthermore, as most clusters leave the simulation box by collision with NA, this effect is the main factor for the large cluster formation potential. The main NA collisions pathways $(SA)_2(base)_2+(NA)_1$ and $(SA)_1(NA)_1(base)_2+(NA)_1$ were disabled as allowed outgoing clusters for the NA−SA−TMA and NA−SA−DMA systems to probe the effect of this collision. For the NA−SA−TMA system, the cluster formation potential was reduced to 0.545 and 23.1 cm^{-3} s^{-1} in the lower and upper concentration limit regimes, respectively, which corresponds to an enhancement rate of 1.01 and 1.05. The lower concentration limit system no longer contains outgoing clusters with NA, and for the upper concentration limit, only 7% contain NA via the $(SA)_2(base)_2+(NA)_1(base)_1$ pathway. For the NA−SA−DMA system, the cluster formation potential reduced to 0.518 and 8.47 cm^{-3} s^{-1} in the lower and upper concentration limit regimes, respectively, which corresponds to an enhancement rate of 1.03 and 1.27. The lower limit system no longer contains outgoing clusters with NA, and for the upper concentration limit distribution, only 9% of the flux contains NA via the $(NA)_2(base)_2+(NA)_1$ pathway. Furthermore, these small enhancements are only present for concentrations of NA between $2.46 \times 10^{10} - 2.46 \times 10^{11}$ molecules cm^{-3}. NA is, therefore, still able to enhance the cluster formation potential, albeit at a much lower efficiency, and the effect quickly drops off when lowering the concentration of NA. However, when NA is present in high concentrations together with SA or MSA, such as in polluted Chinese megacities at coastal regions, NA will likely contribute to new particle formation.

4. CONCLUSIONS

The thermodynamics and cluster formation potentials were calculated for $(acid)_{1-2}$ $(base)_{1-2}$ and $(acid)_3(base)_2$ clusters containing at least one nitric acid (NA) with either sulfuric acid (SA) or methanesulfonic acid (MSA) and bases. The bases studied were ammonia (A), methylamine (MA), dimethylamine (DMA), trimethylamine (TMA), and ethylenediamine (EDA). The calculations were done at the DLPNO−CCSD(T$_0$)/aug-cc-pVTZ//ωB97X-D/6-31++G-(d,p) level of theory with the quasi-harmonic approximation at 298.15 K, 1 atm, and a cutoff of 100 cm^{-1}. We find that the cluster structures resemble their non-NA-containing counterparts and that the clusters lowest in binding free energy contain SA and combinations of strong bases. At smaller cluster sizes, the lowest binding free energy roughly scales with basicity, but at larger sizes, an affinity for DMA/EDA is found, and a disfavor for TMA appears because of sterical hindrance and hydrogen-bond capacity becoming a dominating factor. At the $(acid)_1(base)_2$ cluster size there is a preference, in terms of addition free energy, for adding NA to MSA clusters compared with adding NA to SA clusters, but this effect dissipates at larger sizes. Cluster dynamics simulations show that the cluster formation potential of SA−base and MSA−base clusters are enhanced up to a factor of 88 compared with their non-NA counterparts for relevant grow paths. We find that the NA−SA−DMA, NA−SA−TMA and NA−SA−EDA clusters show the highest cluster formation potential. Hence, these clusters are potential candidates to be extended to larger sizes in future work.

As NA has been shown to greatly enhance the cluster formation potential, we will in the following manuscript in the series study other abundant acid molecules that could stabilize the initial cluster formation. For example, formic acid is another acid found in high concentrations that has been shown to be the most efficient organic acid in enhancing MSA−MA cluster formation.[84] Formic acid has furthermore been shown to be just as effective as ammonia in stabilizing small clusters containing sulfuric acid, formic acid, ammonia, and water.[85] Hence, further studies on the role of formic acid in cluster formation are warranted.

■ ASSOCIATED CONTENT

Ⓢ Supporting Information

The Supporting Information is available free of charge at https://pubs.acs.org/doi/10.1021/acsomega.2c04278.

> Structures of the 10 lowest free energy $(acid)_3(base)_2$ cluster systems. The clusters leaving the simulation box, contributing to $J_{potential}$ (PDF)

> XYZ files of the five lowest free energy cluster configurations for each system, identified at the ωB97X-D/6-31++G(d,p) level of theory (ZIP)

■ AUTHOR INFORMATION

Corresponding Author

Jonas Elm − *Department of Chemistry, iClimate, Aarhus University, 8000 Aarhus C, Denmark;* ⓞ orcid.org/0000-0003-3736-4329; Phone: +45 28938085; Email: jelm@chem.au.dk

Author

Yosef Knattrup − *Department of Chemistry, Aarhus University, 8000 Aarhus C, Denmark;* ⓞ orcid.org/0000-0003-3549-7494

Complete contact information is available at:
https://pubs.acs.org/10.1021/acsomega.2c04278

Notes

The authors declare no competing financial interest.

■ REFERENCES

(1) Haywood, J.; Boucher, O. Estimates of the Direct and Indirect Radiative Forcing due to Tropospheric Aerosols: A Review. *Rev. Geophys.* **2000**, *38*, 513−543.

(2) Lohmann, U.; Feichter, J. Global Indirect Aerosol Effects: A Review. *Atmos. Phys. Chem.* **2005**, *5*, 715−737.

(3) Merikanto, J.; Spracklen, D. V.; Mann, G. W.; Pickering, S. J.; Carslaw, K. S. Impact of Nucleation on Global CCN. *Atmos. Chem. Phys.* **2009**, *9*, 8601−8616.

(4) IPCC. *Climate Change 2021: The Physical Science Basis. Contribution of Working Group I to the Sixth Assessment Report of the Intergovernmental Panel on Climate Change*; Masson-Delmotte, V., Zhai, P., Pirani, A., Connors, S.L.; Péan, C., Berger, S.; Caud, N.; Chen, Y.; Goldfarb, L.; Gomis, M.I.; Huang, M.; Leitzell, K.; Lonnoy, E.; Matthews, J.B.R.; Maycock, T.K.; Waterfield, T.; Yelekçi, O., Yu, R., Zhou, B., Eds.; Cambridge University Press: Cambridge, United Kingdom and New York, 2021. DOI: 10.1017/9781009157896.

(5) Sipilää, M.; Berndt, T.; Petäjä, T.; Brus, D.; Vanhanen, J.; Stratmann, F.; Patokoski, J.; Mauldin, R. L.; Hyvärinen, A.-P.; Lihavainen, H.; Kulmala, M. The Role of Sulfuric Acid in Atmospheric Nucleation. *Science* **2010**, *327*, 1243−1246.

(6) Kirkby, J.; Curtius, J.; Almeida, J.; Dunne, E.; Duplissy, J.; Ehrhart, S.; Franchin, A.; Gagne, S.; Ickes, L.; Kürten, A.; et al. Role of Sulphuric Acid, Ammonia and Galactic Cosmic Rays in Atmospheric Aerosol Nucleation. *Nature* **2011**, *476*, 429−433.

(7) Kulmala, M.; Kontkanen, J.; Junninen, H.; Lehtipalo, K.; Manninen, H. E.; Nieminen, T.; Petäjä, T.; Sipilä, M.; Schobesberger, S.; Rantala, P.; et al. Direct Observations of Atmospheric Aerosol Nucleation. *Science* **2013**, *339*, 943−946.

(8) Schobesberger, S.; Junninen, H.; Bianchi, F.; Lönn, G.; Ehn, M.; Lehtipalo, K.; Dommen, J.; Ehrhart, S.; Ortega, I. K.; Franchin, A.; et al. Molecular Understanding of Atmospheric Particle Formation from Sulfuric Acid and Large Oxidized Organic Molecules. *Proc. Natl. Acad. Sci. U.S.A.* **2013**, *110*, 17223−17228.

(9) Elm, J. Clusteromics I: Principles, Protocols and Applications to Sulfuric Acid - Base Cluster Formation. *ACS Omega* **2021**, *6*, 7804−7814.

(10) Elm, J. Clusteromics II: Methanesulfonic Acid-Base Cluster Formation. *ACS Omega* **2021**, *6*, 17035−17044.

(11) Seinfeld, J. H.; Pandis, S. N. *Atmospheric Chemistry and Physics from Air Pollution to Climate Change*; Wiley: New York, 3rd ed., 2016.

(12) Acker, K.; Möller, D.; Auel, R.; Wieprecht, W.; Kalaß, D. Concentrations of Nitrous acid, Nitric acid, Nitrite and Nitrate in the Gas and Aerosol Phase at a Site in the Emission Zone During ESCOMPTE 2001 Experiment. *Atmos. Res.* **2005**, *74*, 507−524.

(13) Yan, J.; Jung, J.; Zhang, M.; Xu, S.; Lin, Q.; Zhao, S.; Chen, L. Significant Underestimation of Gaseous Methanesulfonic Acid (MSA) over Southern Ocean. *Environ. Sci. Technol.* **2019**, *53*, 13064−13070.

(14) Baccarini, A.; Karlsson, L.; Dommen, J.; Duplessis, P.; Vüllers, J.; Brooks, I. M.; Saiz-Lopez, A.; Salter, M.; Tjernström, M.; et al. Frequent New Particle Formation Over the High Arctic Pack Ice by Enhanced Iodine Emissions. *Nat. Commun.* **2020**, *11*, 4924.

(15) Beck, L. J.; Sarnela, N.; Junninen, H.; Hoppe, C. J. M.; Garmash, O.; Bianchi, F.; Riva, M.; Rose, C.; Peräkylä, O.; Wimmer, D.; et al. Differing Mechanisms of New Particle Formation at Two Arctic Sites. *Geophys. Res. Lett.* **2021**, *48*, No. e2020GL091334.

(16) Wang, M.; Kong, W.; Marten, R.; He, X.-C.; Chen, D.; Pfeifer, J.; Heitto, A.; Kontkanen, J.; Dada, L.; Kürten, A.; et al. Rapid Growth of New Atmospheric Particles by Nitric Acid and Ammonia Condensation. *Nature* **2020**, *581*, 184−189.

(17) Wang, M.; Xiao, M.; Bertozzi, B.; Marie, G.; Rörup, B.; Schulze, B.; Bardakov, R.; He, X.-C.; Shen, J.; Scholz, W.; et al. Synergistic HNO$_3$−H$_2$SO$_4$−NH$_3$ Upper Tropospheric Particle Formation. *Nature* **2022**, *605*, 483−489.

(18) Liu, L.; Yu, F.; Du, L.; Yang, Z.; Francisco, J. S.; Zhang, X. Rapid Sulfuric Acid-dimethylamine Nucleation Enhanced by Nitric Acid in Polluted Regions. *Proc. Natl. Acad. Sci. U.S.A.* **2021**, *118*, No. e2108384118.

(19) Passananti, M.; Zapadinsky, E.; Zanca, T.; Kangasluoma, J.; Myllys, N.; Rissanen, M. P.; Kurtén, T.; Ehn, M.; Attoui, M.; Vehkamäki, H. How Well Can We Predict Cluster Fragmentation Inside a Mass Spectrometer? *Chem. Commun.* **2019**, *55*, 5946−5949.

(20) Zapadinsky, E.; Passananti, M.; Myllys, N.; Kurtén, T.; Vehkamäki, H. Modeling on Fragmentation of Clusters inside a Mass Spectrometer. *J. Phys. Chem. A* **2019**, *123*, 611−624.

(21) Kurtén, T.; Sundberg, M. R.; Vehkamäki, H.; Noppel, M.; Blomqvist, J.; Kulmala, M. Ab Initio and Density Functional Theory Reinvestigation of Gas-Phase Sulfuric Acid Monohydrate and Ammonium Hydrogen Sulfate. *J. Phys. Chem. A* **2006**, *110*, 7178−7188.

(22) Kurtén, T.; Torpo, L.; Sundberg, M. R.; Kerminen, V.; Vehkamäki, H.; Kulmala, M. Estimating the NH$_3$:H$_2$SO$_4$ Ratio of Nucleating Clusters in Atmospheric Conditions using Quantum Chemical Methods. *Atmos. Chem. Phys.* **2007**, *7*, 2765−2773.

(23) Torpo, L.; Kurtén, T.; Vehkamäki, H.; Laasonen, K.; Sundberg, M. R.; Kulmala, M. Significance of Ammonia in Growth of Atmospheric Nanoclusters. *J. Phys. Chem. A* **2007**, *111*, 10671−10674.

(24) Kurtén, T.; Loukonen, V.; Vehkamäki, H.; Kulmala, M. Amines are Likely to Enhance Neutral and Ion-induced Sulfuric Acid-water Nucleation in the Atmosphere More Effectively than Ammonia. *Atmos. Chem. Phys.* **2008**, *8*, 4095−4103.

(25) Nadykto, A. B.; Yu, F.; Jakovleva, M. V.; Herb, J.; Xu, Y. Amines in the Earth's Atmosphere: A Density Functional Theory Study of the Thermochemistry of Pre-Nucleation Clusters. *Entropy* **2011**, *13*, 554−569.

(26) Herb, J.; Nadykto, A. B.; Yu, F. Large Ternary Hydrogen-bonded Pre-nucleation Clusters in the Earth's Atmosphere. *Chem. Phys. Lett.* **2011**, *518*, 7−14.

(27) Ortega, I. K.; Kupiainen, O.; Kurtén, T.; Olenius, T.; Wilkman, O.; McGrath, M. J.; Loukonen, V.; Vehkamäki, H. From Quantum Chemical Formation Free Energies to Evaporation Rates. *Atmos. Chem. Phys.* **2012**, *12*, 225−235.

(28) Nadykto, A. B.; Herb, J.; Yu, F.; Xu, Y. Enhancement in the Production of Nucleating Clusters due to Dimethylamine and Large Uncertainties in the Thermochemistry of Amine-Enhanced Nucleation. *Chem. Phys. Lett.* **2014**, *609*, 42−49.

(29) DePalma, J. W.; Doren, D. J.; Johnston, M. V. Formation and Growth of Molecular Clusters Containing Sulfuric Acid, Water, Ammonia, and Dimethylamine. *J. Phys. Chem. A* **2014**, *118*, 5464−5473.

(30) Nadykto, A. B.; Herb, J.; Yu, F.; Xu, Y.; Nazarenko, E. S. Estimating the Lower Limit of the Impact of Amines on Nucleation in the Earth's Atmosphere. *Entropy* **2015**, *17*, 2764−2780.

(31) Elm, J. Elucidating the Limiting Steps in Sulfuric Acid - Base New Particle Formation. *J. Phys. Chem. A* **2017**, *121*, 8288−8295.

(32) Elm, J.; Passananti, M.; Kurtén, T.; Vehkamäki, H. Diamines Can Initiate New Particle Formation in the Atmosphere. *J. Phys. Chem. A* **2017**, *121*, 6155−6164.

(33) Myllys, N.; Kubečka, J.; Besel, V.; Alfaouri, D.; Olenius, T.; Smith, J. N.; Passananti, M. Role of Base Strength, Cluster Structure and Charge in Sulfuric Acid-Driven Particle Formation. *Atmos. Chem. Phys.* **2019**, *19*, 9753−9768.

(34) Chen, D.; Li, D.; Wang, C.; Liu, F.; Wang, W. Formation Mechanism of Methanesulfonic Acid and Ammonia Clusters: A Kinetics Simulation Study. *Atmos. Environ.* **2020**, *222*, 117161.

(35) Chen, D.; Li, D.; Wang, C.; Luo, Y.; Liu, F.; Wang, W. Atmospheric Implications of Hydration on the Formation of Methanesulfonic Acid and Methylamine Clusters: A Theoretical Study. *Chemosphere* **2020**, *244*, 125538.

(36) Shen, J.; Xie, H.; Elm, J.; Ma, F.; Chen, J.; Vehkamäki, H. Methanesulfonic Acid-driven New Particle Formation Enhanced by Monoethanolamine: A Computational Study. *Environ. Sci. Technol.* **2019**, *53*, 14387−14397.

(37) Dawson, M. L.; Varner, M. E.; Perraud, V.; Ezell, M. J.; Gerber, R. B.; Finlayson-Pitts, B. J. Simplified Mechanism for New Particle Formation from Methanesulfonic Acid, Amines, and Water Via Experiments and Ab Initio Calculations. *Proc. Natl. Acad. Sci. U.S.A.* **2012**, *109*, 18719−18724.

(38) Chen, H. H.; Ezell, M. J.; Arquero, K. D.; Varner, M. E.; Dawson, M. L.; Gerber, R. B.; Finlayson-Pitts, B. J. New Particle Formation and Growth from Methanesulfonic Acid, Trimethylamine and Water. *Phys. Chem. Chem. Phys.* **2015**, *17*, 13699−13709.

(39) Chen, H. H.; Varner, M. E.; Gerber, R. B.; Finlayson-Pitts, B. J. Reactions of Methanesulfonic Acid with Amines and Ammonia as a Source of New Particles in Air. *J. Phys. Chem. B* **2016**, *120*, 1526−1536.

(40) Chen, H. H.; Finlayson-Pitts, B. J. New Particle Formation from Methanesulfonic Acid and Amines/ammonia as a Function of Temperature. *Environ. Sci. Technol.* **2017**, *51*, 243−252.

(41) Arquero, K. D.; Gerber, R. B.; Finlayson-Pitts, B. J. The Role of Oxalic Acid in New Particle Formation from Methanesulfonic Acid, Methylamine, and Water. *Environ. Sci. Technol.* **2017**, *51*, 2124−2130.

(42) Arquero, K. D.; Xu, J.; Gerber, R. B.; Finlayson-Pitts, B. J. Particle Formation and Growth from Oxalic Acid, Methanesulfonic Acid, Trimethylamine and Water: A Combined Experimental and Theoretical Study. *Phys. Chem. Chem. Phys.* **2017**, *19*, 28286−28301.

(43) Shen, J.; Elm, J.; Xie, H.; Chen, J.; Niu, J.; Vehkamäki, H. Structural Effects of Amines in Enhancing Methanesulfonic Acid-Driven New Particle Formation. *Environ. Sci. Technol.* **2020**, *54*, 13498−13508.

(44) Perraud, V.; Xu, J.; Gerber, R. B.; Finlayson-Pitts, B. J. Integrated Experimental and Theoretical Approach to Probe the Synergistic Effect of Ammonia in Methanesulfonic Acid Reactions with Small Alkylamines. *Environ. Sci.: Process. Impacts* **2020**, *22*, 305−328.

(45) Chen, D.; Wang, W.; Li, D.; Wang, W. Atmospheric Implication of Synergy in Methanesulfonic Acid−base Trimers: A Theoretical Investigation. *RSC Adv.* **2020**, *10*, 5173−5182.

(46) Nguyen, M.-T.; Jamka, A. J.; Cazar, R. A.; Tao, F.-M. Structure and Stability of the Nitric Acid−ammonia Complex in the Gas Phase and in Water. *J. Chem. Phys.* **1997**, *106*, 8710−8717.

(47) Tao, F.-M. Gas Phase Proton Transfer Reaction of Nitric Acid-ammonia and the Role of Water. *J. Chem. Phys.* **1998**, *108*, 193−202.

(48) Ling, J.; Ding, X.; Li, Z.; Yang, J. First-Principles Study of Molecular Clusters Formed by Nitric Acid and Ammonia. *J. Phys. Chem. A* **2017**, *121*, 661−668.

(49) Besel, V.; Kubečka, J.; Kurtén, T.; Vehkamäki, H. Impact of Quantum Chemistry Parameter Choices and Cluster Distribution Model Settings on Modeled Atmospheric Particle Formation Rates. *J. Phys. Chem. A* **2020**, *124*, 5931−5943.

(50) Kumar, M.; Li, H.; Zhang, X.; Zeng, X. C.; Francisco, J. S. Nitric Acid−Amine Chemistry in the Gas Phase and at the Air−Water Interface. *J. Am. Chem. Soc.* **2018**, *140*, 6456−6466.

(51) Liu, L.; Li, H.; Zhang, H.; Zhong, J.; Bai, Y.; Ge, M.; Li, Z.; Chen, Y.; Zhang, X. The Role of Nitric Acid in Atmospheric New Particle Formation. *Phys. Chem. Chem. Phys.* **2018**, *20*, 17406−17414.

(52) Elm, J. Clusteromics III: Acid Synergy in Sulfuric Acid-Methanesulfonic Acid-Base Cluster Formation. *ACS Omega* **2022**, *7*, 15206−15214.

(53) Frisch, M. J.; Trucks, G. W.; Schlegel, H. B.; Scuseria, G. E.; Robb, M. A.; Cheeseman, J. R.; Scalmani, G.; Barone, V.; Petersson, G. A.; Nakatsuji, H.et al. *Gaussian 16*, Revision A.03; Gaussian, Inc., Wallingford, CT, 2016.

(54) Stewart, J. J. P. Optimization of Parameters for Semiempirical Methods VI: More Modifications to the NDDO Approximations and Re-optimization of Parameters. *J. Mol. Model.* **2013**, *19*, 1−32.

(55) Elm, J. An Atmospheric Cluster Database Consisting of Sulfuric Acid, Bases, Organics, and Water. *ACS Omega* **2019**, *4*, 10965−10974.

(56) Neese, F. *WIREs Comput. Mol. Sci.* **2012**, *2*, 73−78.

(57) Neese, F. Software update: the ORCA program system, version 4.0. *WIREs Comput. Mol. Sci.* **2017**, *8* (1), e1327.

(58) Riplinger, C.; Neese, F. An Efficient and Near Linear Scaling Pair Natural Orbital Based Local Coupled Cluster Method. *J. Chem. Phys.* **2013**, *138*, 034106.

(59) Riplinger, C.; Sandhoefer, B.; Hansen, A.; Neese, F. Natural Triple Excitations in Local Coupled Cluster Calculations with Pair Natural Orbitals. *J. Chem. Phys.* **2013**, *139*, 134101.

(60) Liakos, D. G.; Sparta, M.; Kesharwani, M. K.; Martin, J. M. L.; Neese, F. Exploring the Accuracy Limits of Local Pair Natural Orbital Coupled-Cluster Theory. *J. Chem. Theory. Comput.* **2015**, *11*, 1525−1539.

(61) Chai, J.; Head-Gordon, M. Long-Range Corrected Hybrid Density Functionals with Damped Atom-Atom Dispersion Corrections. *Phys. Chem. Chem. Phys.* **2008**, *10*, 6615−6620.

(62) Elm, J.; Mikkelsen, K. V. Computational Approaches for Efficiently Modelling of Small Atmospheric Clusters. *Chem. Phys. Lett.* **2014**, *615*, 26−29.

(63) Myllys, N.; Elm, J.; Kurtén, T. Density Functional Theory Basis Set Convergence of Sulfuric Acid-Containing Molecular Clusters. *Comp. Theor. Chem.* **2016**, *1098*, 1−12.

(64) Elm, J.; Bilde, M.; Mikkelsen, K. V. Assessment of Binding Energies of Atmopsheric Clusters. *Phys. Chem. Chem. Phys.* **2013**, *15*, 16442−16445.

(65) Elm, J.; Kristensen, K. Basis Set Convergence of the Binding Energies of Strongly Hydrogen-Bonded Atmospheric Clusters. *Phys. Chem. Chem. Phys.* **2017**, *19*, 1122−1133.

(66) Schmitz, G.; Elm, J. Assessment of the DLPNO binding energies of strongly non-covalent bonded atmospheric molecular clusters. *ACS Omega* **2020**, *5*, 7601−7612.

(67) Grimme, S. Supramolecular Binding Thermodynamics by Dispersion-corrected Density Functional Theory. *Chem. Eur. J.* **2012**, *18*, 9955−9964.

(68) Funes-Ardois, I.; Paton, R. S. *GoodVibes: GoodVibes v1.0.1*, ver. *1.0.1*. GitHub, 2016. DOI: 10.5281/zenodo.60811.

(69) Temelso, B.; Morrison, E. F.; Speer, D. L.; Cao, B. C.; Appiah-Padi, N.; Kim, G.; Shields, G. C. Effect of Mixing Ammonia and Alkylamines on Sulfate Aerosol Formation. *J. Phys. Chem. A* **2018**, *122*, 1612−1622.

(70) Kubečka, J.; Besel, V.; Kurtén, T.; Myllys, N.; Vehkamäki, H. Configurational Sampling of Noncovalent (Atmospheric) Molecular Clusters: Sulfuric Acid and Guanidine. *J. Phys. Chem. A* **2019**, *123*, 6022−6033.

(71) Odbadrakh, T. T.; Gale, A. G.; Ball, B. T.; Temelso, B.; Shields, G. C. Computation of Atmospheric Concentrations of Molecular Clusters from ab initio Thermochemistry. *J. Vis. Exp.* **2020**, *158*, No. e60964.

(72) Elm, J.; Kubečka, J.; Besel, V.; Jääskeläinen, M. J.; Halonen, R.; Kurtén, T.; Vehkamäki, H. Modeling the Formation and Growth of Atmospheric Molecular Clusters: A Review. *J. Aerosol. Sci.* **2020**, *149*, 105621.

(73) Zhang, J.; Dolg, M. ABCluster: The Artificial Bee Colony Algorithm for Cluster Global Optimization. *Phys. Chem. Chem. Phys.* **2015**, *17*, 24173−24181.

(74) Zhang, J.; Dolg, M. Global Optimization of Clusters of Rigid Molecules using the Artificial Bee Colony Algorithm. *Phys. Chem. Chem. Phys.* **2016**, *18*, 3003−3010.

(75) Temelso, B.; Mabey, J. M.; Kubota, T.; Appiah-Padi, N.; Shields, G. C. ArbAlign: A Tool for Optimal Alignment of Arbitrarily

Ordered Isomers Using the Kuhn−Munkres Algorithm. *J. Chem. Inf. Model* **2017**, *57*, 1045−1054.

(76) Kildgaard, J. V.; Mikkelsen, K. V.; Bilde, M.; Elm, J. Hydration of Atmospheric Molecular Clusters: A New Method for Systematic Configurational Sampling. *J. Phys. Chem. A* **2018**, *122*, 5026−5036.

(77) Kildgaard, J. V.; Mikkelsen, K. V.; Bilde, M.; Elm, J. Hydration of Atmospheric Molecular Clusters II: Organic Acid-Water Clusters. *J. Phys. Chem. A* **2018**, *122*, 8549−8556.

(78) McGrath, M. J.; Olenius, T.; Ortega, I. K.; Loukonen, V.; Paasonen, P.; Kurtén, T.; Kulmala, M.; Vehkamäki, H. Atmospheric Cluster Dynamics Code: A Flexible Method for Solution of the Birth-Death Equations. *Atmos. Chem. Phys.* **2012**, *12*, 2345−2355.

(79) Olenius, T.; Kupiainen-Määttä, O.; Ortega, I. K.; Kurtén, T.; Vehkamäki, H. Free Energy Barrier in the Growth of Sulfuric Acid-Ammonia and Sulfuric Acid-Dimethylamine Clusters. *J. Chem. Phys.* **2013**, *139*, 084312.

(80) *Atmospheric Cluster Dynamics Code.* https://github.com/tolenius/ACDC (accessed 2021-11-01).

(81) Roldin, P.; Ehn, M.; Kurtén, T.; Olenius, T.; Rissanen, M. P.; Sarnela, N.; Elm, J.; Rantala, P.; Hao, L.; Hyttinen, N.; et al. The Role of Highly Oxygenated Organic Molecules in the Boreal Aerosol-cloud-climate System. *Nat. Commun.* **2019**, *10*, 4370.

(82) Hunter, E. P. L.; Lias, S. G. Evaluated Gas Phase Basicities and Proton Affinities of Molecules: An Update. *J. Phys. Chem. Ref. Data* **1998**, *27*, 413.

(83) Xie, H. B.; Elm, J. Tri-Base Synergy in Sulfuric Acid-Base Clusters. *Atmosphere* **2021**, *12*, 1260.

(84) Zhang, R.; Shen, J.; Xie, H.-B.; Chen, J.; Elm, J. The Role of Organic Acids in New Particle Formation from Methanesulfonic Acid and Methylamine. *Atmos. Chem. Phys.* **2022**, *22*, 2639−2650.

(85) Harold, S. E.; Bready, C. J.; Juechter, L. A.; Kurfman, L. A.; Vanovac, S.; Fowler, V. R.; Mazaleski, G. E.; Odbadrakh, T. T.; Shields, G. C. Hydrogen-Bond Topology Is More Important Than Acid/Base Strength in Atmospheric Prenucleation Clusters. *J. Phys. Chem. A* **2022**, *126*, 1718−1728.